Digital Signal Processing 50 (2016) 191–202

Contents lists available at ScienceDirect

Digital Signal Processing

www.elsevier.com/locate/dsp

DOA estimation in conformal arrays based on the nested array principles

Pourya Alinezhad, Saeid R. Seydnejad *, Dariush Abbasi-Moghadam

Department of Electrical Engineering, Shahid Bahonar University of Kerman, Kerman, Iran

ARTICLE INFO

Article history:
Available online 4 January 2016

Keywords:
Conformal array
Nested array
DOA estimation
MUSIC

ABSTRACT

The nested array structure has attracted great attention recently due to its ability in reducing the number of sensors in an array and at the same time preserving the array performance. While a uniform linear array (ULA) can detect at most $N-1$ sources with N sensors, a nested array can provide $O(N^2)$ degrees of freedom with the same number of sensors; allowing us to detect K sources with $K > N$ sensors. Direction of arrival (DOA) estimation in a conformal array is a challenging task. In this article, by breaking the conformal array into smaller sub-arrays and using an interpolation technique, we employ the nested array principles to detect more number of sources than sensors. This comes at the cost of more snapshots and lower resolution, in the DOA estimation of an arbitrarily-shaped conformal array. Each sub-array in the conformal array is selected such that the "shadow effect" which leads to an incomplete steering vector in the DOA estimation algorithm is eliminated. The selected sub-arrays are then transformed to virtual nested arrays where more degrees of freedom can be obtained by applying the MUSIC algorithm for DOA estimation. The application of our proposed method is highlighted by considering a set of comprehensive examples for cylindrical and spherical arrays.

1. Introduction

A conformal antenna array is an array with its antennas conformed to its bearing surface. Due to this flexibility, conformal arrays have found great applications in many modern defense and wireless communication systems [1,2]. Unfortunately, the existing beamforming and direction-of-arrival (DOA) estimation algorithms which have been developed for conventional planar arrays cannot be directly applied to conformal arrays since these algorithms assume elements with identical patterns which is not valid in conformal arrays. Due to the curvature of the bearing surface, each element in a conformal array has a far-field contribution in the direction of the incident signals which is different from the contributions of other elements. This means that, unlike conventional planar arrays, one cannot separate the element pattern from the array factor in the analysis of a conformal array [1]. To use high resolution DOA estimation algorithms such as MUSIC [3] or ESPRIT [4] for arrays with arbitrary geometries, interpolation techniques have been employed by some authors [5–13]. The interpolation technique is a method which enables us to map an array with M sensors to an array with $N \geq M$ virtual sensors. The manifold matrix of a non-uniform planar array is, in general, not Vandermonde. By using array interpolation, a virtual uniform planar array is generated which ensures obtaining a Vandermonde matrix. Particularly, in [13] a DOA estimation method for conformal arrays is proposed which uses the interpolation technique to transform a conformal array into a uniform linear array (or a uniform planar array). By applying LS-ESPRIT, 2D-DFT ESPRIT and MUSIC algorithms to the interpolated array the authors in [13] have shown that this method can identify the DOA of different sources with great accuracy for different conformal array geometries. Array interpolation has also been applied to both narrowband and wideband signals [5–11].

The number of signals that can be detected by conventional arrays is always less than the number of array sensors, e.g. an array with N sensors can resolve at most $N-1$ sources [14]. However, in many applications, while the size of the array is limited, it is required to detect more number of signals than the number of elements. Such examples can be found, for example, in Unmanned Aerial Vehicles (UAV). UAVs are highly mobile units that can be employed as safe and efficient communication relays for various surveillance, reconnaissance, and other tactical missions [15]. While increasing the degrees of freedom (DOF) in the array of a UAV can increase its performance, the physical size and the weight of the array is a limiting factor.

* Corresponding author.
E-mail address: sseydnejad@uk.ac.ir (S.R. Seydnejad).

http://dx.doi.org/10.1016/j.dsp.2015.12.009
1051-2004/

Different methods have been proposed so far in order to increase the DOF of conventional arrays [16–20]. A large number of such methods use the sparse array structure [16–20]. A sparse array is a uniform array where certain fractions of its elements have been removed randomly. A sparse array has a large variation in its peak sidelobe level. Hence, optimization techniques must be used to remove appropriate elements to have a good sidelobe behavior [16–18]. These sparse arrays, also called thinned arrays, are designed under specific considerations such as a particular radiation pattern or impedance matching of the array elements [19,20].

Minimum redundancy arrays (MRA) constitute a sub-group of sparse arrays, which use the idea of co-array design to increase the DOF [21–24]. Co-array theory is based on the fact that the difference of element positions in an array structure appears in the signal correlation matrix [25]. MRAs provide more DOF both by reducing the number of elements and by manipulating the received signals in order to extract the missing data of the removed elements. The main drawback of the minimum redundancy arrays is that they do not have a closed form expression for the array geometry and the achievable DOF.

Another group of sparse arrays, the so-called co-prime array, was proposed and developed in [26,27], using $N_{c1} + N_{c2}$ sensors to obtain $O(N_{c1}N_{c2})$ degrees of freedom for DOA estimation where N_{c1} and N_{c2} are co-prime numbers. In co-prime arrays, two separate ULAs with element spacing dN_{c1} and dN_{c2} are placed together on a row where the difference of the element positions forms a uniform spatial sampling with the aid of the co-array theory.

The newly proposed structure, namely the nested array, can overcome the issues of the MRAs and at the same time can achieve $O(N^2)$ degrees of freedom using N sensors by combining two or more Uniform Linear Arrays (ULA) with increasing inter-element spacing [28]. Furthermore, compared to a co-prime array, a nested array requires less number of sensors to achieve the same DOF. By using the co-array theory, a nested array can achieve more DOF but it is at the cost of lower detection resolution compared to conventional methods with the same number of snapshots because the finite sample size of the signals can have more negative impact on the accuracy of the covariance matrix in a nested array than a conventional array. This is an inherent problem of nested arrays and has also been reported in previous literature [28,29].

This issue has been mitigated recently by exploiting the numerous iterations of subsets of the whole data set in both nested arrays and co-prime arrays [30]. Due to these prominent features, the nested array structure has been recently extended from one-dimensional arrays to two-dimensional arrays [29,31] and from narrowband sources to wideband signals [32].

Our aim in this article is to increase the DOF in the DOA estimation of a conformal array to detect more number of sources than the sensors, thereby improving the performance of a conformal array. For this purpose, we map the given conformal array to a corresponding linear or planar nested array using the interpolation technique. First, the desired spatial angle in the conformal array is divided into small sectors to reduce the interpolation error and eliminate the shadow effect. The shadow effect appears when some of the elements of the conformal array are not able to receive the incoming signals due to the curvature of the arrays. Each sector is then transformed, by means of an appropriate transformation matrix, into a corresponding virtual nested array. This transformation is also applied to the impinging signals on the conformal array. Next the conventional high resolution DOA estimation algorithms can be applied to each virtual nested array to provide more DOF. Selecting the size of each sub-array and the number of elements in its corresponding nested array are design parameters that determine the accuracy of the DOA estimation. In summary, our approach includes two steps: a) a transformation from conformal geometry to a virtual linear (planar) array geometry, b) increasing the DOF by applying the nested array principle to this virtual linear (planar) array.

The organization of the paper is as follows. The next section briefly reviews the nested array principles and its associated spatial smoothing technique and shows how this structure can increase the DOF in both 1D (linear) and 2D (planar) arrays. In section 3, the "shadow effect" problem in a conformal array is discussed. Section 4 presents our approach to develop the nested array structure to a conformal array and shows how the detected number of sources can be increased in the DOA estimation based on this new design. Simulation results are presented in Section 5 for a cylindrical conformal array as a typical example for the 1D case and a spherical conformal array as a typical example for the 2D case. Finally, Section 6 concludes the paper.

2. Nested array principles

Nested arrays are a subgroup of sparse arrays and use the co-array theory to increase the DOF. Since the distribution of the sensors in a nested array is non-uniform, we need to first consider the signal model in a non-uniform 1D (linear) array.

We will use bold lowercase and uppercase characters to denote vectors and matrices, respectively. The symbol $(.)^*$ denotes the conjugate operator, $(.)^{\mathrm{T}}$ the transpose operator, and $(.)^{\mathrm{H}}$ the conjugate transpose operator. N is used for the number of sensors in a nested array and M is used for the number of sensors in a conformal array. Since in our case, the nested array is a virtual array whereas the conformal array is the actual (physical) array we use two different symbols for referring to their sensors.

2.1. Non-uniform linear array

Consider an N element non-uniform linear antenna array. Let $\mathbf{a}(\theta)$ denote the $N \times 1$ steering vector corresponding to the direction θ defined as [28],

$$\mathbf{a}(\theta) = \left[e^{j(\frac{2\pi}{\lambda})d_1 \sin\theta}\ e^{j(\frac{2\pi}{\lambda})d_2 \sin\theta} \dots\ e^{j(\frac{2\pi}{\lambda})d_N \sin\theta}\right]^{\mathrm{T}} \tag{1}$$

where d_i denotes the position of the ith sensor and λ is the signal wavelength. Suppose that D narrowband sources are impinging on this array from directions $\{\theta_d, d = 1, 2, \dots, D\}$ with powers $\{\sigma_d^2, d = 1, 2, \dots, D\}$, respectively. We can write the received signal model as [28],

$$\mathbf{y}(t) = \mathbf{A}\mathbf{x}(t) + \mathbf{e}(t) \tag{2}$$

where $\mathbf{y}(t) = [y_1(t)\ y_2(t) \dots y_N(t)]^{\mathrm{T}}$ is the vector of the received signals, $\mathbf{A} = [\mathbf{a}(\theta_1)\ \mathbf{a}(\theta_2) \dots \mathbf{a}(\theta_D)]$ is an $N \times D$ matrix which represents the array manifold, and $\mathbf{x}(t) = [s_1(t)\ s_2(t) \dots s_D(t)]^{\mathrm{T}}$ denotes the source signal vector. The impinging signals are assumed to be uncorrelated with each other. The channel noise $\mathbf{e}(t)$ is assumed to be temporally and spatially white and uncorrelated from the source with the covariance of $\sigma_e^2\mathbf{I}$. From (2), the autocorrelation matrix $\mathbf{R_{yy}} = E[\mathbf{y}\mathbf{y}^{\mathrm{H}}]$ of the received signal is written as [28],

$$\mathbf{R_{yy}} = \mathbf{A}\mathbf{R_{xx}}\mathbf{A}^{\mathrm{H}} + \sigma_e^2\mathbf{I} = \mathbf{A}\mathbf{\Lambda}\mathbf{A}^{\mathrm{H}} + \sigma_e^2\mathbf{I} \tag{3}$$

where $\mathbf{R_{xx}}$ represents the covariance matrix of the sources, $\mathbf{\Lambda}$ is a diagonal matrix with signal powers at its diagonal elements and $\mathbf{I}$ denotes the identity matrix.

2.2. 1D nested array structure

A simple 1D nested array is a non-uniform linear array consisting of two concatenated ULAs as it is shown in Fig. 1 [28]. With N sensors, the first ULA has N_1 sensors with interelement spacing $d_1 = \lambda/2$ and the second ULA has N_2 sensors with interelement spacing $d_2 = (N_1 + 1)d_1$ [28].

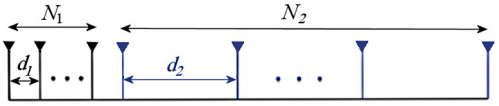

Fig. 1. A nested array with N_1 sensors in the first ULA and N_2 sensors in the second ULA with d_1 and d_2 interelement spacings, respectively.

By vectorizing $\mathbf{R_{yy}}$ in (3) we get [28,33],

$$\mathbf{z} = \mathrm{vec}(\mathbf{R_{yy}}) = \mathrm{vec}\left[\sum_{i=1}^{D} \sigma_i^2 \big(\mathbf{a}(\theta_i)\mathbf{a}^{\mathrm{H}}(\theta_i)\big)\right] + \sigma_e^2 \mathbf{i}' = \big(\mathbf{A}^* * \mathbf{A}\big)\mathbf{p} + \sigma_e^2 \mathbf{i}' \tag{4}$$

where $\mathbf{p} = [\sigma_1^2\ \sigma_2^2 \dots \sigma_D^2]^{\mathrm{T}}$ and $\mathbf{i}' = [\mathbf{e}_1^{\mathrm{T}}\ \mathbf{e}_2^{\mathrm{T}} \dots \mathbf{e}_N^{\mathrm{T}}]^{\mathrm{T}}$ with $\mathbf{e}_i$ being a column vector of all zeros except a 1 at the ith position. Equation (4) is the signal model for a 1D nested array. By comparing (4) with (2) we can conclude that $\mathbf{z}$ in (4) behaves like the received signal of an array whose manifold is given by $(\mathbf{A}^* * \mathbf{A})$ [28]. The symbol $*$ denotes the Khatri–Rao product between two matrices of appropriate sizes [33]. The Khatri–Rao product $(\mathbf{A}^* * \mathbf{A})$ in (4) gives rise to the notion of the difference co-array and provides the required DOF produced by the nested array structure.

2.2.1. Co-array principle

The "difference co-array" is defined as an array with the positions of its elements chosen from the set $\pm\{(m-n)d; 1 \le m \le N, 1 \le n \le N\}$. To elaborate on this definition, assume a narrowband signal $s(t)$ with the wavelength λ impinging on a uniform linear array from the direction θ. Then, the received signal at the nth sensor will be given by [28],

$$y_n(t) = e^{j\frac{2\pi}{\lambda} nd \sin\theta} s(t) \tag{5}$$

Consequently, the cross-correlation between the signals received at the nth and mth sensors will be,

$$\mathrm{E}\big[y_m(t) y_n^*(t)\big] = e^{j\frac{2\pi}{\lambda}((m-n)d)\sin\theta} \sigma_d^2 \tag{6}$$

It can be seen that the term $v \triangleq (m-n)$ appears in the exponent of the cross-correlation function. The hypothetical elements placed on the $(v \times d)$ positions are called the "difference co-array" of the given array. Obviously, this difference can be produced by different sensors in the array. This is called redundancy [28].

The manifold matrix $\mathbf{A}$ and its conjugate $\mathbf{A}^*$ in the nested array equation of (4) contains the terms $\exp(j(2\pi/\lambda)d_m \sin\theta_d)$ and $\exp(-j(2\pi/\lambda)d_n \sin\theta_d)$, respectively where d_i denotes the position of the ith sensor. Therefore, the product $(\mathbf{A}^* * \mathbf{A})$ will contain the terms with the difference of the element positions $\exp(-j(2\pi/\lambda)(d_m - d_n)\sin\theta_d)$ and it will behave like the manifold matrix of a (longer) hypothetical array whose sensor locations are given by distinct values in the set $\{d_m - d_n; 1 \le m \le N, 1 \le n \le N\}$ [28].

Although the model in (4) provides more DOF, the vector $\mathbf{p}$ contains only scalar values as if we are dealing with coherent signals. Therefore, appropriate techniques should be invoked to eliminate this coherent nature of the signal model in (4). Spatial smoothing is a well-known technique for the arrays dealing with coherent signals and it is briefly discussed below in the context of the nested array structure.

2.2.2. Spatial smoothing technique

Spatial smoothing method is a popular technique to deal with coherent signals [34,35]. The spatial smoothing technique can be applied to the nested array signal model of (4) after removing the redundancies of difference co-array of the nested array which will result a virtual ULA with $(N^2/2 + N + 1)$ elements. Hence, by choosing $L = (N^2/4 + N/2)$ sub-arrays with size $h = (N^2/4 + N/2)$ on this virtual ULA the spatial smoothing method could be implemented as [28],

$$\mathbf{R_{ss}} = \frac{1}{\frac{N^2}{4} + \frac{N}{2}} \sum_{i=1}^{\frac{N^2}{4}+\frac{N}{2}} \mathbf{R}_i \tag{7}$$

in which $\mathbf{R}_i$ is the corresponding covariance matrix of the ith sub-array in the difference co-array of the nested array. It can be proved that (7) is equivalent to [28],

$$\mathbf{R_{ss}} = \frac{1}{\frac{N^2}{4} + \frac{N}{2}} \big(\mathbf{A}_1 \mathbf{\Lambda} \mathbf{A}_1^{\mathrm{H}} + \sigma_e^2 \mathbf{I}\big)^2 \tag{8}$$

In (8) $\mathbf{A}_1$ represents the manifold matrix of the first sub-array with $h = (N^2/4 + N/2)$ elements and is given by [28],

$$\mathbf{A}_1 = \begin{bmatrix} 1 & 1 & 1 \\ a_1 & \dots & a_D \\ \vdots & \ddots & \vdots \\ a_1^{(N^2/4+N/2-1)} & \dots & a_D^{(N^2/4+N/2-1)} \end{bmatrix} \tag{9}$$

where $a_i = e^{j\frac{2\pi}{\lambda} d \sin\theta_i}$. $\mathbf{A}_1$ is obviously a Vandermonde matrix.

The spatially smoothed matrix $\mathbf{R_{ss}}$ enables us to perform the detection of $(N^2/4 + N/2 - 1)$ sources with N sensors which is obviously of $O(N^2)$ degrees. However, the finite-sample effect will destroy the Toeplitz structure of $\mathbf{R_{ss}}$; the algorithm with spatial smoothing will not converge to the optimum solution any more. This causes degradation in the resolution of DOA estimation. By eigendecomposition of $\mathbf{R_{ss}}$ its corresponding eigenvalues will span the null space of $\mathbf{A}_1$. Therefore, by using (8) we can conduct the DOA estimation with higher DOF for the coherent signal model of (4).

2.3. 2D nested array

A two dimensional (planar) nested array uses the same principles of the one dimensional (linear) nested array. However, the theory of 2D nested array is much more complicated than its 1D counterpart. The 2D nested array has more co-array configurations, sophisticated sensor placement routines and it also suffers from the "identifiability issue" which happens in 2D DOA estimation problems [29]. In the following, we will briefly describe the element positioning procedure in the 2D plane and develop a signal model for the 2D nested array.

2.3.1. 2D nested array structure

In order to illustrate a 2D nested array, we should first define lattices which contain array elements. A planar lattice is constructed by using a 2×2 non-singular generator matrix $\mathbf{V} = [\mathbf{v}_1\ \mathbf{v}_2]$ where $\mathbf{v}_1$ and $\mathbf{v}_2$ are 2×1 vectors [31]. If we place the array elements on the tip of the arrows (vectors) and their shifted replicas, then the corresponding lattice of the generator matrix $\mathbf{V}$ is constructed as it is shown in Fig. 2(a).

A 2D nested array structure consists of the union of the sensors on two lattices. One dense lattice, with the generator matrix $\mathbf{N}^{(\mathrm{d})}$, and another sparse lattice with the generator matrix $\mathbf{N}^{(\mathrm{s})}$. An arbitrary 2×2 integer matrix $\mathbf{P}$ determines the relation between the dense and the sparse lattices as $\mathbf{N}^{(\mathrm{s})} = \mathbf{N}^{(\mathrm{d})}\mathbf{P}$ [31]. We define the $FPD(\mathbf{P})$ (Fundamental Parallelepiped) of the matrix $\mathbf{P}$ as the area contained in the parallelepiped whose sides are given by the two column vectors of $\mathbf{P}$ as it is shown in Fig. 2(a) [31].

The dense array has $N^{(\mathrm{d})} = \det(\mathbf{P})$ elements on the lattice generated by $\mathbf{N}^{(\mathrm{d})}$ and its sensor locations are given by $\{\mathbf{N}^{(\mathrm{d})}\mathbf{n}^{(\mathrm{d})}, \mathbf{n}^{(\mathrm{d})} \in$

$FPD(\mathbf{P})\}$ where $\mathbf{n}^{(\mathrm{d})}$ is a vector containing all integer vectors in $FPD(\mathbf{P})$ [31]. The sparse array has $N^{(\mathrm{s})}$ elements on the lattice generated by $\mathbf{N}^{(\mathrm{s})}$ with sensor locations given by $\mathbf{N}^{(\mathrm{s})}[n_1^{(\mathrm{s})}\ n_2^{(\mathrm{s})}]^{\mathrm{T}}$ where $0 \le n_1^{(\mathrm{s})} \le N_1^{(\mathrm{s})} - 1$, $0 \le n_2^{(\mathrm{s})} \le N_2^{(\mathrm{s})} - 1$ and $N_1^{(\mathrm{s})} \times N_2^{(\mathrm{s})} = N^{(\mathrm{s})}$ [31]. As an example, Fig. 2(a) shows a nested array with a randomly generated matrix $\mathbf{N}^{(\mathrm{d})}$ and $\mathbf{P} = \left[\begin{smallmatrix} 3 & 1 \\ 3 & 3 \end{smallmatrix}\right]$.

This means that the dense array has $N^{(\mathrm{d})} = \det(\mathbf{P}) = 6$ sensors and $N^{(\mathrm{s})} = 12$. Therefore, the sparse array has 12 sensors located on the sparse lattice generated by $\mathbf{N}^{(\mathrm{s})} = \mathbf{N}^{(\mathrm{d})}\mathbf{P}$. The cross

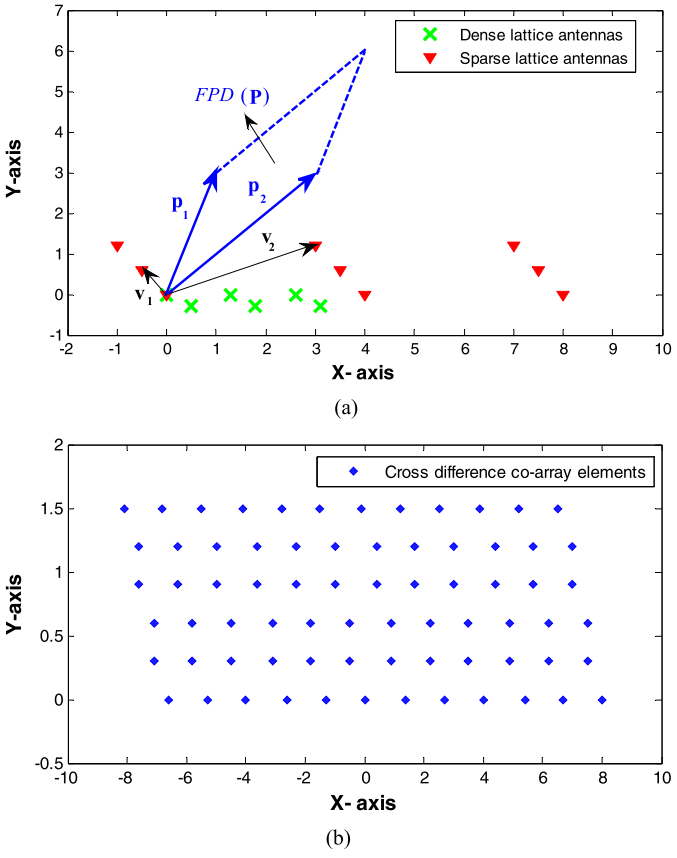

Fig. 2. (a) A 2D nested array with 6 sensors on the dense lattice and 12 sensors on the sparse lattice with the corresponding generator matrix $\mathbf{V} = [\mathbf{v}_1\ \mathbf{v}_2]$ and the fundamental parallelepiped of the matrix $\mathbf{P}$, $FPD(\mathbf{P})$, (b) its corresponding cross difference co-array elements.

difference co-array elements between the sparse and dense lattices are given by $\mathbf{N}^{(\mathrm{s})}\mathbf{n}^{(\mathrm{s})} - \mathbf{N}^{(\mathrm{d})}\mathbf{n}^{(\mathrm{d})}$, $\mathbf{n}^{(\mathrm{s})} \in FPD(\mathbf{N}^{(\mathrm{s})})$ as it is shown in Fig. 2(b). Obviously, the cross difference co-array between the sparse and the dense array results in a planar array with more sensors and this provides more DOF.

We can derive the signal model of the 2D nested array similar to the 1D case as [29],

$$\mathbf{z}_{2\mathrm{D}} = \begin{pmatrix} \mathbf{A}_{\mathrm{s}} \\ \mathbf{A}_{\mathrm{d}} \end{pmatrix}^{*} * \begin{pmatrix} \mathbf{A}_{\mathrm{s}} \\ \mathbf{A}_{\mathrm{d}} \end{pmatrix} \mathbf{p} + \sigma_{\mathrm{e}}^2 \mathbf{I} \tag{10}$$

where $\mathbf{A}_{\mathrm{d}}$ with size $\det(\mathbf{P}) \times D$ and $\mathbf{A}_{\mathrm{s}}$ with size $N^{(\mathrm{s})} \times D$ are manifold matrices corresponding to the dense and the sparse array, respectively [29]. It can be shown that applying 2D spatial smoothing on the coherent signal model of (10) with $h = (N^{(\mathrm{d})} + 1)(N^{(\mathrm{s})} + 1)/4$ sub-arrays of size $L = ((N^{(\mathrm{d})} - 1)/2) \times ((N^{(\mathrm{s})} - 1)/2)$ yields [29],

$$\mathbf{R}_{\mathrm{ss,2D}} = \frac{1}{(N^{(\mathrm{d})} + 1)(N^{(\mathrm{s})} + 1)/4} \times \left(\mathbf{A}_{1,2\mathrm{D}} \mathbf{\Lambda}_{2\mathrm{D}} \mathbf{A}_{1,2\mathrm{D}}^{\mathrm{H}} + \sigma_{\mathrm{e}}^2 \mathbf{I}_{\frac{(N^{(\mathrm{d})}+1)}{2} \times \frac{(N^{(\mathrm{s})}+1)}{2}}\right)^2 \tag{11}$$

where $\mathbf{\Lambda}_{2\mathrm{D}}$ contains signal powers after spatial smoothing. Similar to $\mathbf{A}_1$ in (9), the matrix $\mathbf{A}_{1,2\mathrm{D}}$ is the first sub-array manifold matrix in the 2D nested array [29]. By employing a 2D nested array we can now detect $O(N^{(\mathrm{d})}N^{(\mathrm{s})})$ uncorrelated sources using only $O(N^{(\mathrm{d})} + N^{(\mathrm{s})})$ physical sensors [29].

3. Shadow effect problem

Due to the curvature of a conformal array, a condition may occur in which some of the directional signals may not be received by all antennas. This effect, which is called the "shadow effect", will result in an incomplete steering vector. To have a better view, consider the cylindrical conformal array with $M = 32$ elements shown in Fig. 3. It is obvious that only elements 8 to $M - 8 = 24$ in this array can receive the signal impinging on the array; other elements are blind to this signal. For this array the steering vector can be written as [13],

$$\tilde{\mathbf{a}}\left(\frac{\pi}{2}\right) = \left[1, e^{jkr\cos(\frac{\pi}{2} - \frac{2\pi}{32})}, e^{jkr\cos(\frac{\pi}{2} - \frac{2\times 2\pi}{32})}, e^{jkr\cos(\frac{\pi}{2} - \frac{3\times 2\pi}{32})}, \ldots, 0, \ldots, 0\right]^{\mathrm{T}} \tag{12}$$

where r is the radius of the cylinder and k is the wave number. Equation (12) shows an incomplete steering vector in which the

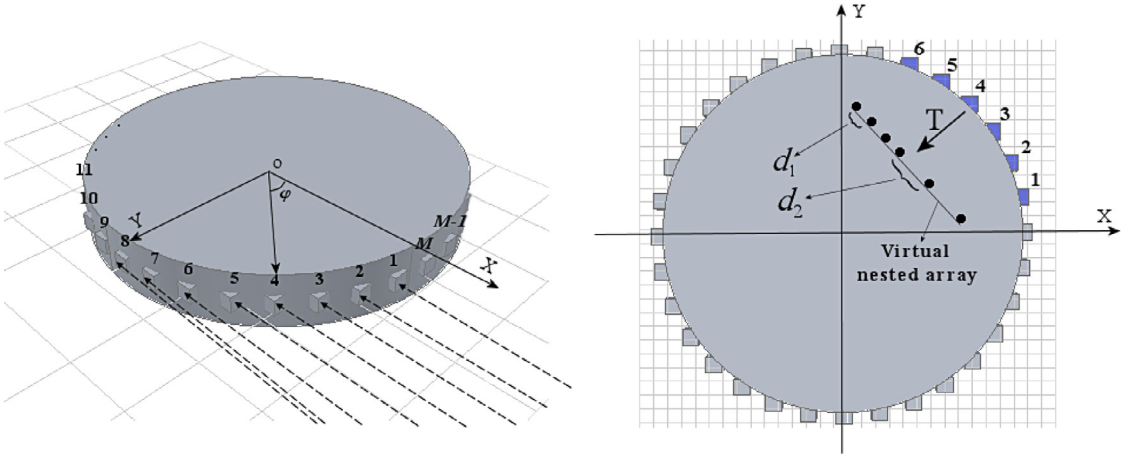

Fig. 3. (a) A cylindrical conformal array showing the shadow effect, (b) conformal array and virtual nested arrays. Antennas 1 to 6 are mapped to a virtual nested array.

number of zeros is equal to the number of the elements which are blind to the signal. This incomplete steering vector will cause many problems in high performance DOA algorithms. The DOA estimation algorithms will encounter estimation error with an incomplete steering vector. In order to overcome the problem of the incomplete steering vector and simultaneously increase the DOF, we break the conformal array into several sub-arrays and apply the interpolation technique to each sub-array. The selection of each sub-array is such that it only deals with the sources of its own view angle. Therefore, there is no shadow effect for this sub-array. The combination of all sub-arrays covers all the impinging sources.

4. The proposed method

In the proposed method, we first describe how to break the conformal array into several sub-arrays. Each sub-array corresponds to a spatial sector. Then we use the interpolation technique to map each sub-array to a virtual nested array and apply the MUSIC algorithm to each nested array.

4.1. Array interpolation

To eliminate the incomplete steering vector we should divide the conformal array into J sub-arrays. Using this notion we can always find a sub-array whose elements can receive the signal with a complete steering vector (no shadow effect) and apply the standard MUSIC algorithm as,

$$\mathbf{P}_{\text{MUSIC}}(\varphi) = \frac{1}{\mathbf{a}_c^{\text{H}}(\varphi)\mathbf{U}_{\text{N}}\mathbf{U}_{\text{N}}^{\text{H}}\mathbf{a}_c(\varphi)} \tag{13}$$

in which $\mathbf{a}_c$ denotes the complete steering vector. It is worthwhile noting that for a typical conformal array the field of view of each sector should not be larger than $\pi/2$ to prevent the shadow effect [12]. The interpolation technique can now be applied to each sub-array. This means that each sub-array corresponds to a sector (field of view) of the entire space. For example, in Fig. 3(b) for the first sub-array, the searching sector could be from π/M to $12\pi/M$. If there is a signal whose DOA is in the sector $\Phi = [\varphi_1, \varphi_2]$ where φ_1 and φ_2 are the left and right boundaries of this sector and we choose $\Delta\varphi$ as the interpolation step and n as the interpolation number, then Φ can be represented as,

$$\Phi = \left[\varphi_1, \varphi_1 + \Delta\varphi, \varphi_1 + 2\Delta\varphi, \ldots, \varphi_1 + (n-1)\Delta\varphi, \varphi_2\right] \tag{14}$$

Since each element in a conformal array has a different normal direction, the response of each element will be different to an incident wave from others. Therefore, we must consider antenna element responses together with the array manifold matrix. If the number of elements in this sector is denoted by $\bar{L}$, then the conformal array manifold matrix will be given by,

$$\mathbf{F} \odot \bar{\mathbf{A}}(\varphi_1, \varphi_2) = \left[\mathbf{f}(\varphi_1) \odot \bar{\mathbf{a}}(\varphi_1), \mathbf{f}(\varphi_1 + \Delta\varphi) \odot \bar{\mathbf{a}}(\varphi_1 + \Delta\varphi), \ldots, \mathbf{f}(\varphi_2) \odot \bar{\mathbf{a}}(\varphi_2)\right] \tag{15}$$

in which $\odot$ represents the Hadamard multiplication, $\mathbf{F}$ is an $\bar{L} \times K$ beampattern matrix which contains the response of the $\bar{l}$th antenna $\{\bar{l} = 1, \ldots, \bar{L}\}$ to the kth signal, $k = \{1, \ldots, K\}$, $\bar{\mathbf{A}}$ is a $\bar{L} \times K$ manifold matrix whose columns are the steering vectors of the K signals on the conformal array, and we define,

$$\mathbf{f}(\varphi_i) = \left[f(\varphi_i - \beta_1), f(\varphi_i - \beta_2), \ldots, f(\varphi_i - \beta_{\bar{L}})\right]^{\text{T}} \tag{16}$$

in (16) $f(\varphi_i - \beta_{\bar{l}})$ represents the element pattern of the $\bar{l}$th antenna in the direction of φ_i and β is added to consider spatial phase shift for different element positions. Equation (15) is now a complete manifold for the sector (i.e. with no zero entries).

In the next step we need to map (15) to the steering vector of the nested array. Suppose that $L \times K$ matrix $\mathbf{A} = [\mathbf{a}(\varphi_1)\ \mathbf{a}(\varphi_2) \ldots \mathbf{a}(\varphi_K)]$ is the manifold matrix for the K impinging signals on an L element nested array. By dividing the nested array field of view between φ_1 and φ_2 we can write,

$$\mathbf{A}(\varphi_1, \varphi_2) = \left[\mathbf{a}(\varphi_1)\ \mathbf{a}(\varphi_1 + \Delta\varphi) \ldots \mathbf{a}(\varphi_2)\right] \tag{17}$$

in which $\mathbf{A}(\varphi_1, \varphi_2)$ is $L \times n$. Fig. 3(b) shows how the above procedure is applied to a cylindrical array. In the proposed method, the physical array with the manifold matrix (15) is mapped to a virtual nested array with the manifold matrix (17) through a transformation matrix $\mathbf{T}$. Thus, we should have,

$$\mathbf{T}^{\text{H}}\left(\mathbf{F} \odot \bar{\mathbf{A}}(\varphi)\right) = \mathbf{A}(\varphi) \quad \varphi \in \mathbf{\Phi} \tag{18}$$

The matrix $\mathbf{T}$ with a size of $\bar{L} \times L$ maps the matrix $(\mathbf{F} \odot \bar{\mathbf{A}}(\varphi))$ over a set of discrete angles $\varphi \in [\varphi_1, \varphi_2]$ and can be obtained by minimizing a norm constrained least squares (LS) error criterion as [9]:

$$\mathbf{t}_i = \arg\min_{\mathbf{t}_i} \left\|\mathbf{A}^{\text{H}}(\varphi)\mathbf{t}_i - (\mathbf{f}_i - \bar{\mathbf{a}}_i)\right\|_2^2 \quad \text{with } \|\mathbf{t}_i\|_2 \le \alpha,\ i = 1, \ldots, \bar{L} \tag{19}$$

where $\mathbf{t}_i$ denotes the ith column of $\mathbf{T}$ and $(\mathbf{f}_i - \bar{\mathbf{a}}_i)$ shows the ith column of $(\mathbf{F} \odot \bar{\mathbf{A}}(\varphi))$. The desired norm constraint in (19) is given by the parameter α. The solution of (19) is obtained with details in [9] and [36]. Other methods have also been proposed to obtain $\mathbf{T}$ [7,37,38]. The accuracy of the interpolation can be examined by comparing the ratio of the Frobenius norm,

$$\varepsilon = \frac{\|\mathbf{A}(\varphi) - \mathbf{T}^{\text{H}}(\mathbf{F} \odot \bar{\mathbf{A}}(\varphi))\|_{\text{F}}}{\|\mathbf{F} \odot \bar{\mathbf{A}}(\varphi)\|_{\text{F}}} \tag{20}$$

Obviously, it is impossible to find an ideal $\mathbf{T}$ to satisfy (18). A large L is desirable for a nested array to further increase the degrees of freedom and decrease ε. On the other hand, increasing L may increase the condition number of $\mathbf{T}$ and produce an ill-conditioned problem [6].

4.2. DOA with 1D nested array

Once an acceptable nested array is obtained, the received signals should also be mapped with the interpolation matrix $\mathbf{T}$. Suppose that the received data vector of the conformal array is denoted by $\mathbf{Y}(t) = [y_1(t)\ y_2(t) \ldots y_M(t)]^{\text{T}}$ and the data vector of the ith sub-array of size $\bar{L}$ is denoted by $\mathbf{Y}_i(t) = [y_{i1}(t) \ldots y_{i\bar{L}}(t)]^{\text{T}}$ then the received signals of the virtual nested array $\mathbf{Z}_i(t)$ are given by,

$$\mathbf{Z}_i(t) = \mathbf{T}_i\mathbf{Y}_i(t), \quad i = 1 : \text{number of subarrays} \tag{21}$$

Now both the virtual nested array and its corresponding received signals are provided and we can use the MUSIC based DOA estimation algorithm and obtain higher DOF. Based on (13) we can obtain the corresponding MUSIC spectrum for each sub-array by substituting the noise subspace derived from the spatial smoothed matrix $\mathbf{R}_{\text{ss}}$ in (8) for the 1D nested array and replace the complete steering vector $\mathbf{a}_c$ by $\mathbf{A}_1$ where $\mathbf{A}_1$ is defined in (9). Therefore, the MUSIC spectrum in every sector of the interpolated 1D nested array associated with the conformal array can be computed as,

$$\mathbf{P}_{\text{MUSIC}}(\varphi_1, \varphi_2) = \frac{1}{\mathbf{A}_1^{\text{H}}(\varphi_1, \varphi_2)\mathbf{U}_{\text{N}}\mathbf{U}_{\text{N}}^{\text{H}}\mathbf{A}_1(\varphi_1, \varphi_2)} \tag{22}$$

The noise subspace matrix $\mathbf{U}_N$ is derived from decomposition of $\mathbf{R}_{ss}$ in (8) which is the nested array correlation matrix with the size $(L^2/4 + L/2) \times (L^2/4 + L/2)$ for a sub-array. This enables us to perform the DOA estimation with higher degrees of freedom to explore $(L^2/4 + L/2 - 1)$ signals with L elements on the virtual nested array.

4.3. DOA with 2D nested array

A 2D interpolation is needed in order to transform the array elements of a conformal array to the 2D nested array. Other steps are taken similar to a 1D nested array. For 2D interpolation, (14) can be replaced by,

$$[\Phi, \Theta] = \big[(\varphi_1, \theta_1), (\varphi_1 + \Delta\varphi, \theta_1 + \Delta\theta), \ldots, \big(\varphi_1 + (K_1 - 1)\Delta\varphi, \theta_1 + (K_2 - 1)\Delta\theta\big), (\varphi_2, \theta_2)\big] \quad (23)$$

where K_1 is the interpolation number in the φ direction and K_2 is the interpolation number in the θ direction. Obviously, a 2D array needs much more interpolation points than a 1D array. In a similar manner, the noise subspace matrix $\mathbf{U}_N$ can be derived from the eigendecomposition of $\mathbf{R}_{ss,2D}$ in (11) for the 2D nested array. Hence, in the 2D case the formula of the MUSIC spectrum for each sector can be written as,

$$\mathbf{P}_{MUSIC}(\Phi, \Theta) = \frac{1}{\mathbf{A}_{1,2D}^H(\Phi, \Theta)\mathbf{U}_N\mathbf{U}_N^H\mathbf{A}_{1,2D}(\Phi, \Theta)} \quad (24)$$

where $\mathbf{A}_{1,2D}$ denotes the manifold matrix of the first sub-array in spatial smoothing of the 2D nested array.

4.4. The implementation procedure

The processing steps of the proposed algorithm can be summarized as follows. The titles marked as Offline are calculated and stored in the system in the initialization phase and the Online steps are executed in real-time.

INPUTS AND INITIALIZATION (Offline):

1 **Begin:**
- **INPUT:** φ, β (these values are derived from the array geometry)
- **OUTPUT:** Calculate the element pattern matrix $\mathbf{f}$ of the conformal array in (16).

2 Break the conformal array into several sub-arrays to eliminate the shadow effect
- **OUTPUT:** $\bar{L}$, number of sensors of each subarray
- **OUTPUT:** Calculate the steering vector $\bar{\mathbf{a}}(\varphi)$ of each sub-array for (15).

3 Assume a virtual nested array with N elements for each sub-array.
- **OUTPUT:** Calculate steering vector $\mathbf{a}(\varphi)$ of the virtual nested array for (17).

4 Set the interpolation parameters:
- **INPUT:** (φ_1, φ_2) = left and right boundaries of sector Φ,
- **INPUT:** Interpolation step $\Delta\varphi$ (or equivalently $[\Phi, \Theta]$, $\Delta\varphi$ and $\Delta\theta$ for a 2D nested array).
- **INPUT:** The minimum interpolation error ε.

Interpolation (Offline):

5 **Load:** $\mathbf{f}$ and $\bar{\mathbf{a}}(\varphi)$ from steps 1 and 2, respectively.
- **OUTPUT:** Calculate matrix $\mathbf{F} \odot \bar{\mathbf{A}}$ from (15).
- **Load:** $\mathbf{a}(\varphi)$ from step 3.
- **OUTPUT:** Calculate matrix $\mathbf{A}$ from (17)
- **OUTPUT:** Calculate transformation matrix $\mathbf{T}$ in (18) by solving (19).
- **OUTPUT:** Calculate interpolation error ε in (20).

6 **IF** (ε is small enough)
THEN
- **OUTPUT: T**

ELSE IF
- **GOTO step** 2 and choose a different subarray size.

DOA estimation (Online):

7 Use (21) to transform $\mathbf{Y}_i(t)$ to $\mathbf{Z}_i(t)$.
- **LOAD:** $\mathbf{T}$ from step 6.
- **INPUT:** $\mathbf{Y}_i(t)$ (the received data of the conformal array).
- **OUTPUT:** Calculate $\mathbf{Z}_i(t)$ from (21) (the received data of the virtual nested array).

8 Calculate nested array manifold matrix after spatial smoothing
- **LOAD:** $\mathbf{a}(\varphi)$ from step 3.
- **LOAD:** (φ_1, φ_2) from step 4.
- **OUTPUT:** Calculate $\mathbf{A}(\varphi_1, \varphi_2) = [\mathbf{a}(\varphi_1)\mathbf{a}(\varphi_1 + \Delta\varphi)\ldots\mathbf{a}(\varphi_2)]$ in (17).
- **OUTPUT:** Apply nested array theory on $\mathbf{A}(\varphi_1, \varphi_2)$ and derive $\mathbf{A}_1(\varphi_1, \varphi_2)$ in (9).

9 Calculate nested array correlation matrix after spatial smoothing.
- **LOAD:** $\mathbf{Z}_i(t)$ from step 7.
- **ASSIGN:** $\mathbf{x}(t) = \mathbf{Z}_i(t)$ in (2)
- **OUTPUT:** $\mathbf{R}_{ss}$ from (8) ($\mathbf{R}_{ss,2D}$ from (11) in 2D case).

10 Apply (22) for DOA estimation of a 1D nested array or (24) for DOA estimation of a 2D nested array.
- **LOAD:** $\mathbf{R}_{ss}$ from step 9.
- **LOAD:** $\mathbf{A}(\varphi_1, \varphi_2)$ from step 8.
- **OUTPUT:** Calculate $\mathbf{P}_{MUSIC}(\varphi_1, \varphi_2)$ in (22) or $\mathbf{P}_{MUSIC}(\Phi, \Theta)$ in (24).

The above steps are very straightforward for implementation. Importantly, the proposed method can be applied to any conformal array regardless of its geometrical shape.

5. Simulation results

In this section, our proposed method is applied to a cylindrical and a spherical conformal array. For the element response, a microstrip antenna with the following pattern is selected [38].

$$f(\varphi, \theta) = \frac{1}{3}\sin(\theta)\big[1 + 2\max\big(\cos(\varphi), -0.5\big)\big] \quad (25)$$

A microstrip antenna is a good choice for a conformal array due to its unidirectional radiation characteristics [12]. Uncorrelated zero mean random Gaussian processes were assumed for the directional

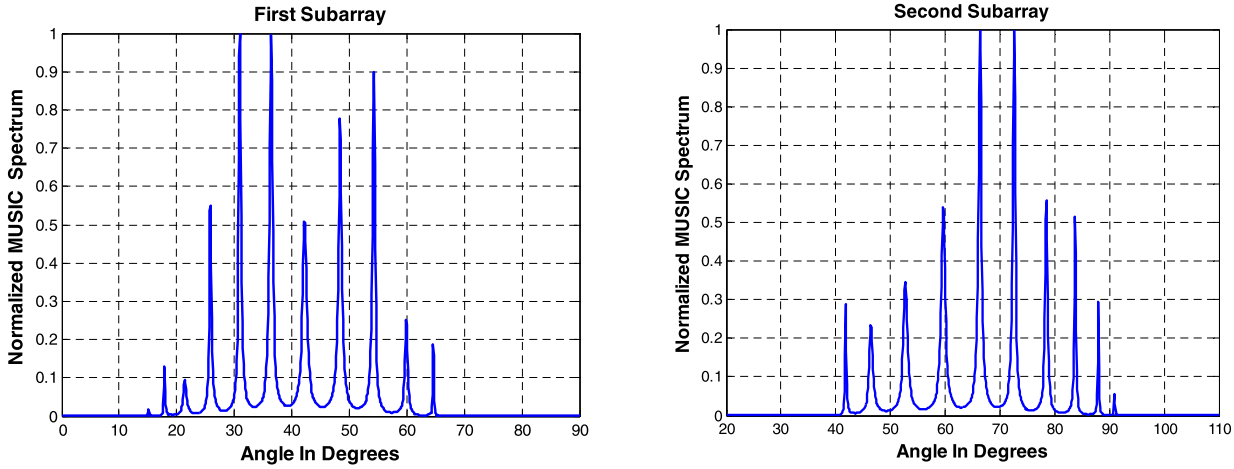

Fig. 4. MUSIC spectrum of, (a) the first sector mapped to a six element nested array, (b) the second sector with some shared sources with the first sector. Both estimated with 1000 snapshots.

sources and the noises were assumed temporally and spatially zero-mean white Gaussian and uncorrelated from the sources with SNR = 10 dB on each antenna.

Five examples are considered here. Example 1 demonstrates the ability of the proposed method to achieve more DOF using 1D nested array structure for a cylindrical array and Example 3 shows the same results for a spherical array using 2D nested array structure. The results of our proposed method are compared with those in [13] for the cylindrical array in Example 2 and for the spherical array in Example 4. Root mean square error (RMSE) versus SNR and the effect of snapshot lengths on the resolution are thoroughly investigated in Example 5.

Example 1. Consider the cylindrical array shown in Fig. 3(a) with radius of $(5/2)\lambda$ and with $M = 32$ microstrip antennas. As it is shown, these antennas are mounted uniformly on the surface of the cylinder in one ring. This array can steer the beam only in the azimuth direction. Consequently, we should handle this conformal array with a 1D nested array.

Assume D narrowband signals $(D > M)$ with azimuth angle φ_i $(i = 1, 2, \ldots, D)$ are impinging on the array. The steering vector of this array is given by $\{\bar{\mathbf{a}}(\varphi_i) = \exp(jkr\cos(\varphi_i - \beta_m)), m = 1, 2, \ldots, M\}$ in which $\beta_m = 2\pi(m-1)/M$ is defined [12]. For a cylindrical array we have $\theta = 90°$ in (25). We choose six elements in each sub-array $(\bar{L} = 6)$. Therefore, the first sector covers the range of $\Phi \in [\pi/32; 12\pi/32]$ with the middle point of the sector is chosen as the reference point. The interpolation step was set to $\Delta\varphi = 0.01$.

Six elements of the physical conformal array are mapped to a six element nested array. The nested array with $L = 6$ could have the total degrees of freedom of $(L^2/4 + L/2 - 1) = 11$ based on (8). We assume that 16 sources with equal powers are impinging on the array and consider 11 sources in the field of the view of the first sector at the directions of $[15°, 18°, 21°, 26°, 31°, 36°, 42°, 48°, 54°, 60°, 65°]$.

Fig. 4(a) shows the MUSIC spectrum obtained by our proposed algorithm. We can clearly see the presence of all sources. Recalling that by using a conformal array mapped to a ULA with six sensors, we can detect only five sources.

We also observe in Fig. 4(a) that the sources which are located at the edges of the sector appear with low amplitudes in the MUSIC spectrum. It is well known that the DOA estimation has better performance for the signals impinging on the array from the normal direction than those impinging closer to the edges. To resolve this issue we apply the DOA estimation to the second sector and select this sector such that the sources far from the normal direction in the first sector are placed close to the normal direction of the second sector. If the second sector of the array is chosen to cover the range of $\Phi = [7\pi/32; 18\pi/32]$ then the sources seen by this sector will be in the set of $[42°, 48°, 54°, 60°, 65°, 72°, 78°, 84°, 88°, 91°]$. The first five sources receiving from the direction of $[42°, 48°, 54°, 60°, 65°]$ are common between the first and the second sectors whereas the rest of the sources can only be seen by this sector. The corresponding MUSIC spectrum for the second sector is plotted in Fig. 4(b). Those sources which were located at the edge of the first sector and could not be estimated well are now estimated properly by the DOA estimation of the second sector.

Example 2. To achieve the same resolution, the nested array needs a larger snapshot than its corresponding ULA [28]. Therefore, it seems necessary to compare our proposed method with a scenario in which a conformal array is mapped to a ULA. In this example the resolution of the proposed algorithm is compared with [13]. We assume three sources impinging on the array from directions $[24°, 25°, 26°]$. Fig. 5(a) shows the MUSIC spectrum for the array considered in Example 1 mapped to a nested array with six elements and Fig. 5(b) shows the same spectrum mapped to a ULA with six elements used in [13], both obtained by 1000 samples. In order to obtain the same sharp peaks a larger snapshot must be used for the nested array. This is shown in Fig. 5(c) for 1500 samples. As it would be expected, increasing the snapshot length has improved the resolution of the DOA estimation.

The accuracy of the transformation matrix $\mathbf{T}$ depends upon the selected angle $\varphi \in [\varphi_1, \varphi_2]$ in (14). Consequently, (20) is used to show how $\mathbf{T}$ affects the interpolation error. Fig. 5(d) shows the interpolation error ε of (20) as a function of the sector length in degrees for both methods. It can be seen that the error for the ULA is less than the nested array. Obviously, the interpolation error is more for the nested array due to its sparse structure. There is, of course, a tradeoff between increasing DOF and the value of ε in the nested array.

Example 3. In this example, we investigate the performance of our proposed algorithm for a spherical conformal array with the radius 2λ as it is shown in Fig. 6(a). It is assumed that 25 elements are placed uniformly on the array over the region $[\varphi = -50° : 50°; \theta = -50° : 50°]$ while 36 narrowband sources

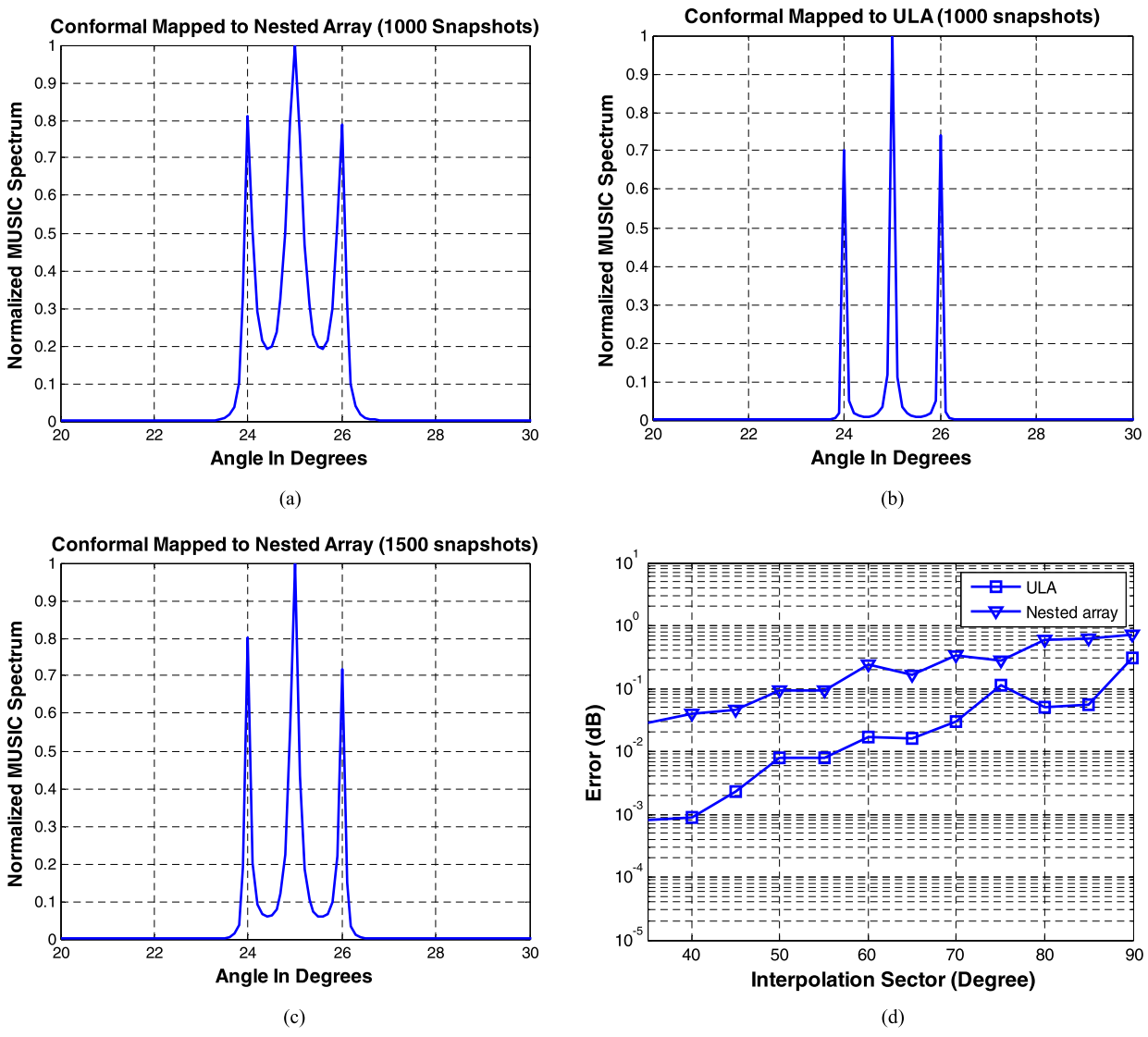

Fig. 5. The MUSIC spectrum of the conformal array mapped to, (a) a virtual nested array with 6 elements estimated with 1000 snapshots, (b) a ULA with 6 elements estimated with 1000 snapshots using the method in [13], (c) a virtual nested array with 6 elements estimated with 1500 snapshots, (d) interpolation error for (a) and (b).

with equal powers are impinging on the array from the angles $\{(\varphi,\theta) = ((\frac{-5\pi}{18} + 2(i-1)\frac{\pi}{18}), (\frac{-5\pi}{18} + 2(k-1)\frac{\pi}{18})), i = 1,\ldots,6, k = 1,\ldots,6\}$. The distribution of the sensors is such that all sources can be considered in one sector for simplicity. This sector is mapped to a 2D nested array with $\mathbf{P} = \left[\begin{smallmatrix} 3 & 0 \\ 0 & 3 \end{smallmatrix}\right]$ and a generator matrix $\mathbf{N}^{(d)} = \left[\begin{smallmatrix} 1 & 0 \\ 0 & 1 \end{smallmatrix}\right]$, which are diagonal matrices. Hence, the dense array has $N^{(d)} = \det(\mathbf{P}) = 9$ elements. Recalling from Section 2 that a non-diagonal matrix constructs a parallelepiped whereas diagonal matrices $\mathbf{P}$ and $\mathbf{N}^{(d)}$ will result in a rectangular 2D nested array because $FPD(\mathbf{P})$ and $FPD(\mathbf{N}^{(d)})$ will be rectangular. This rectangular structure ensures having an interpolation error less than a parallelepiped structure. Moreover, we assume that $N_1^{(s)} = 3$ and $N_2^{(s)} = 6$ thus the sparse array has $N^{(s)} = N_1^{(s)} \times N_2^{(s)} = 18$ elements. Therefore, the nested array will have $N^{(d)} + N^{(s)} = 27$ elements in total.

Fig. 6(b) shows the DOA spectrum obtained by our proposed method. The corresponding contour plot is depicted in Fig. 6(c). It can be seen that the proposed method can effectively detect all sources whereas there is no way to detect the same number of sources by other methods.

The probability of detection of all sources under specific SNR values and snapshot length were studied thoroughly in [29]. Here we have chosen sufficient snapshot length (1000) for the DOA estimation to ensure the detection of all sources. Moreover, in some conditions in the 2D DOA estimation the sources may not be detected properly due to the identifiability issue [29]. In this simulation, the distribution of sources was chosen such that a unique identifiability of sources could be achieved.

Example 4. In this example, we study the resolution of the proposed method for the 2D nested array by comparing its results with its corresponding uniform planar array counterpart proposed in [13].

The advantage of using the nested array method is that it can detect more number of sources than sensors (Fig. 6). For cases where the number of sources is less than the number of sensors both methods can detect all the sources but, as it is shown in this example, the resolution of the conventional method [13] is better than the nested array method with the same length of snapshots. However, when the number of sources becomes more than the number of sensors then a nested array can still detect the sources but the conventional method [13] cannot.

We assume nine narrowband sources with equal powers are impinging on the sub-array chosen in Example 3, where the signal directions are chosen from the pairs of $\{(\varphi,\theta) = ((\frac{-\pi}{18} + 2(i-$

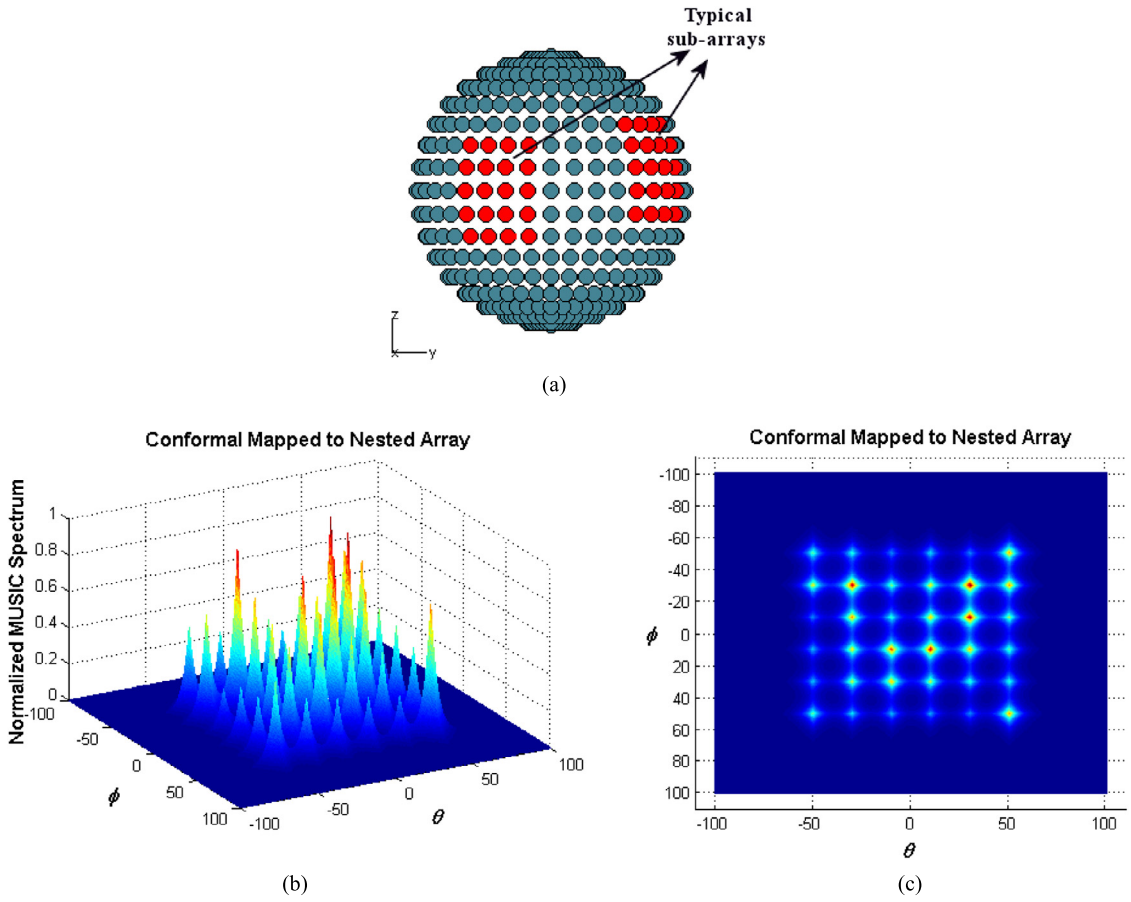

Fig. 6. (a) Spherical conformal array and its typical sub-arrays. (b) MUSIC spectrum using the proposed method with a snapshot with 1000 samples, (c) contour plot of Fig. 6(b).

$1)\frac{\pi}{32}), (\frac{-\pi}{18} + 2(k-1)\frac{\pi}{32})), i = 1, 2, 3, k = 1, 2, 3\}$. The sub-array in the spherical array, which has 25 elements, is mapped to a uniform 2D planar array with 25 elements and a nested array with the same structure as in the previous example with 27 elements.

Figs. 7(a) and (b) show the MUSIC spectrum for both methods and Figs. 7(c) and (d) illustrate their contour plots. Obviously, the nested array could resolve all impinging signals but with relatively lower resolution. Even though the corresponding planar array exhibits higher resolution, it is not able to detect the large number of sources which our method can detect. Similar to the cylindrical array, we can get better resolution in the nested array with larger length of snapshots. This is investigated with more details in the next example.

Example 5. The results of Examples 2 and 4 illustrate that for the same snapshot length the proposed nested based approach provides lower resolution than the method proposed in [13]. In this simulation, we expand our previous results in Examples 2 and 4 and study the RMSE of the angle estimates as a function of both the length of snapshots and signal to noise ratio. We show that increasing the length of snapshots in the proposed method will result in better resolution.

5.1. Cylindrical array

Fig. 8(a) shows the RMSE plots for the array considered in Example 1 mapped to a nested array with six elements and to a ULA with six elements by varying the length of snapshots and SNR = 10 dB for a source at 25°. From Fig. 8(a) we can conclude that by increasing the snapshot length from 500 to 1000 and also from 1000 to 1500 the RMSE value of our proposed method tends to approach to that of the method in [13].

It is worthwhile mentioning that in practice, since the signal correlation matrix is estimated from a finite number of snapshots, the vector $\mathbf{p}$ in (4) is only an approximation to its actual value, hence (8) is derived only approximately and this affects the nested array correlation matrix. However, as it is shown in the numerical example here, even with this approximation the performance of the method is quite satisfactory for a moderate number of snapshots. This point was also concluded in Example 2 (Fig. 5(b) and (c)). Fig. 8(b) shows the RMSE performance versus SNR plot for the same example (snapshots = 1000).

5.2. Spherical array

In this simulation, we plot the RMSE of the proposed method and compare it with the method in [13] for different lengths of snapshots. Fig. 9(a) shows the RMSE plot obtained by averaging over all 9 sources. As it can be seen, the performance of the proposed method improves considerably with a larger length of snapshots. It is clear that for the same length of data there is always a gap between the performance of the two methods. This has also been noted by other authors [28,29] and it is due to the nature of the nested array structure and nothing to do with the method proposed here. This is more obvious in Fig. 9(b) which shows RMSE versus SNR. The same behavior can be seen in Fig. 9(b). For SNR > 0 dB, the RMSE of the method in [13] is almost less than 1.5 degrees but it is almost 2 degrees for the proposed method. Similar to Fig. 9(a) the reason for this difference is due to the finite

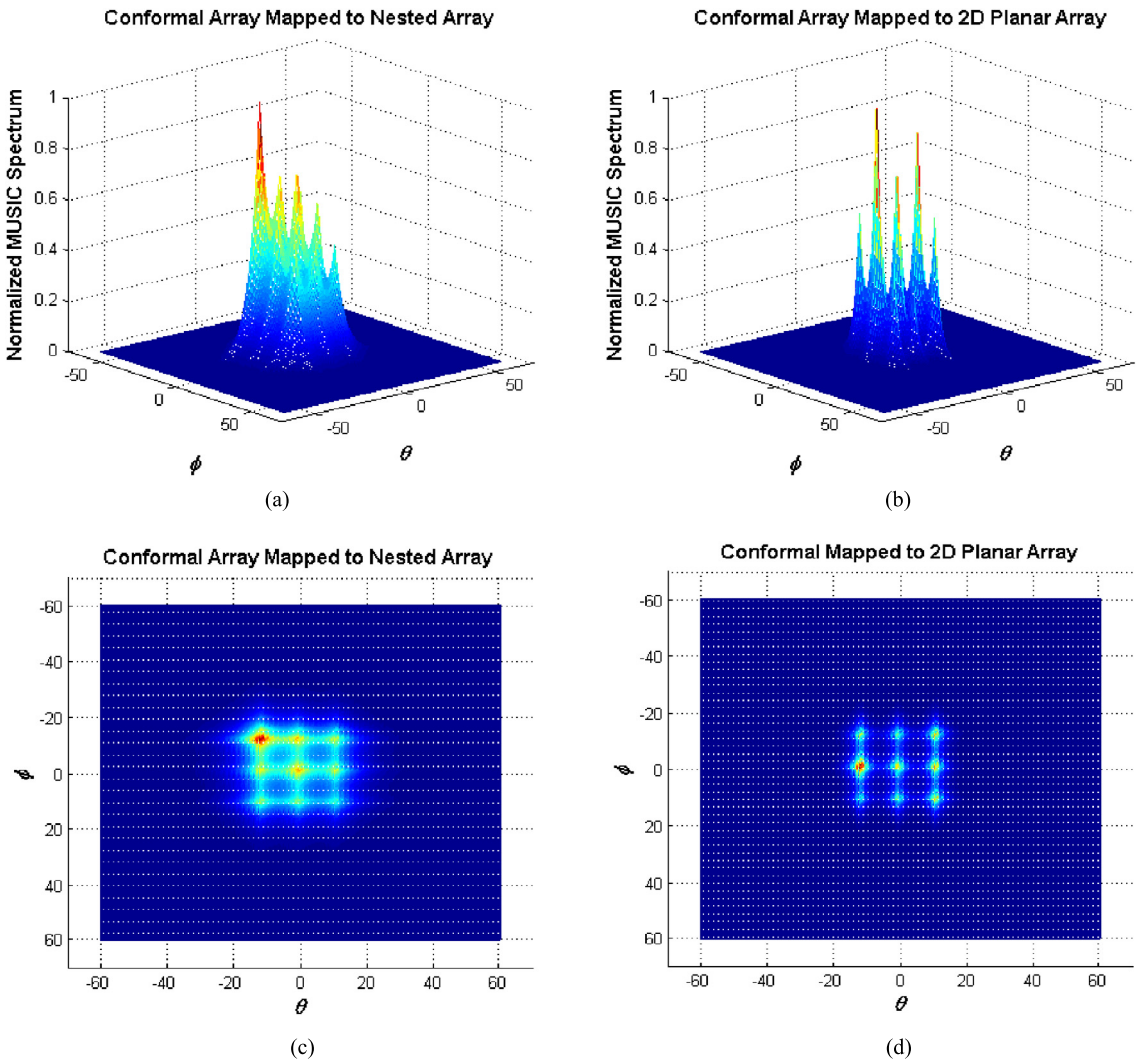

Fig. 7. MUSIC spectrum of the spherical array, (a) mapped to a 2D nested array with 25 elements, (b) mapped to a planar array with 27 elements, (c), (d) their corresponding contour plots.

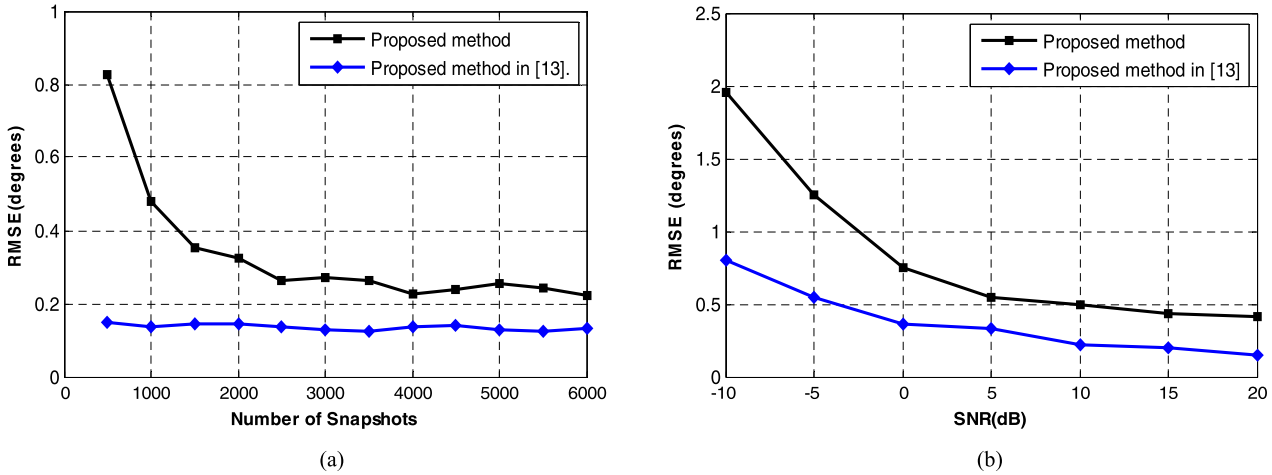

Fig. 8. (a) RMSE (in degrees) versus the length of snapshots for a source at 25° impinging on a cylindrical array for Example 2, (b) RMSE (in degrees) versus SNR for a snapshot with 1000 samples.

length of the snapshots and its impact on the accuracy of the estimation of the correlation matrix in (11). The difference between the performance of the azimuth and elevation angles is because they exhibit different radiation patterns according to (25).

6. Conclusion

In this paper the recently proposed nested array structure was employed to increase the degrees of freedom in the direction of

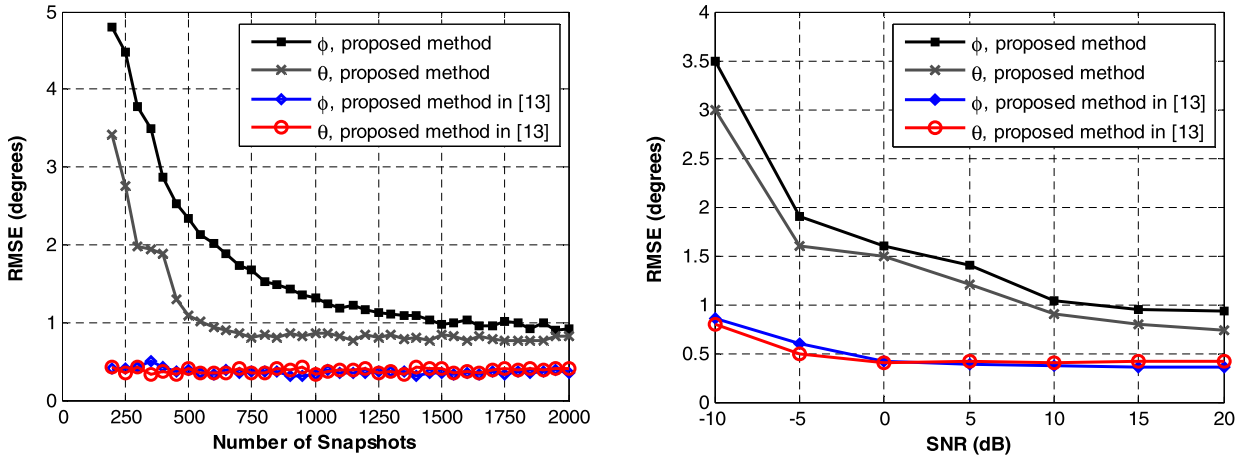

(a) (b)

Fig. 9. (a) RMSE (in degrees) versus the length of snapshot averaged over all 9 sources impinging on a spherical array for Example 4. (b) RMSE (in degrees) versus SNR for a snapshot with 1000 samples.

arrival (DOA) estimation of an arbitrarily-shaped conformal array. By breaking the conformal array into several sub-arrays and transforming each sub-array, using the interpolation technique, to a corresponding virtual nested array we devised a method to detect more number of sources than the sensors. Similar to other nested arrays, this higher number of DOF in the conformal nested array is obtained at the cost of lower resolution compared to conventional methods because the derived formula for the correlation matrix of a nested array needs more number of snapshots in order to be as accurate as the correlation matrix of a conventional array. We applied our method to a typical cylindrical array, which needs 1D nested array analysis, and a typical spherical conformal array, which requires 2D nested array analysis and showed that these higher number of sources can be detected with appropriate resolution. This is a great achievement compared to conventional methods which are limited by the number of sensors for their DOA estimation. Our proposed method can greatly extend the capability of conformal arrays for the applications which are limited by the size of the array and the number of sensors.

References

[1] P. Josefsson, L. Persson, Conformal Array Antenna Theory and Design, IEEE Press Series on Electromagnetic Wave Theory, 2006.
[2] C.A. Balanis, Antenna Theory: Analysis and Design, Wiley, New York, 2005.
[3] R.O. Schmit, Multiple emitter location and signal parameter estimation, IEEE Trans. Antennas Propag. 34 (1986) 276–280.
[4] R. Roy, T. Kailath, ESPRIT-estimation of signal parameters via rotational invariance techniques, IEEE Trans. Acoust. Speech Signal Process. 37 (1989) 984–995.
[5] T.P. Bronez, Sector interpolation of nonuniform arrays for efficient high resolution bearing estimation, in: Proc. IEEE, ICASSP'88, vol. 5, 1988, pp. 2885–2888.
[6] B. Friedlander, The root-MUSIC algorithm for direction finding with interpolated arrays, Signal Process. 30 (1993) 15–29.
[7] M. Pesavento, A.B. Gershman, Z. Luo, Robust array interpolation using second order cone programming, IEEE Signal Process. Lett. 9 (2002) 8–11.
[8] A. Weiss, J.M. Gavish, Direction finding using ESPRIT with interpolated arrays, IEEE Trans. Signal Process. 39 (1991) 1473–1478.
[9] Gerhard Doblinger, Optimized design of interpolated array and sparse array wideband beamformers, in: Proc. EUSIPCO, Lausanne, Switzerland, August 2008, pp. 25–29.
[10] L. Ping'an, Y. Bianzhang, S. Jincai, 2-D spatial-spectrum estimation for wideband sources based on interpolated circular arrays, J. Electron. (China) 13 (1996) 319–324.
[11] M. Johnny, M. Johnny, V.T. Vakili, Wideband direction finding using cumulant with interpolated array, in: IEEE Pacific RIM Conference on Communications, Computers, and Signal Processing – Proceedings, 2011, pp. 135–139.
[12] P. Yang, F. Yang, Z.P. Nie, Robust adaptive beamformer using interpolation technique for conformal antenna array, Prog. Electromagn. Res. 23 (2010) 215–228.
[13] P. Yang, F. Yang, Z.P. Nie, DOA estimation with sub-array divided technique and interpolated esprit algorithm on a cylindrical conformal array antenna, Prog. Electromagn. Res. 103 (2010) 201–216.
[14] H.L.V. Trees, Optimum Array Processing: Part IV of Detection, Estimation and Modulation Theory, Wiley Intersci., New York, 2002.
[15] J.S. Sun, D.S. Gosh, T. Itoh, A sparse conformal retrodirective array for UAV application, in: IEEE MTT-S International Microwave Symposium Digest, 2008, pp. 795–798.
[16] G. Prisco, M. D'Urso, et al., Maximally sparse arrays via sequential convex optimizations, IEEE Antennas Wirel. Propag. Lett. 11 (2012) 192–195.
[17] O.M. Bucci, M. D'Urso, T. Isernia, et al., Deterministic synthesis of uniform amplitude sparse arrays via new density taper techniques, IEEE Trans. Antennas Propag. 58 (2010) 1949–1958.
[18] K. Chen, X. Yun, Z. He, et al., Synthesis of sparse planar arrays using modified real genetic algorithm, IEEE Trans. Antennas Propag. 55 (2007) 1067–1073.
[19] P. Rocca, R.L. Haupt, Dynamic array thinning for adaptive interference cancellation, in: Antennas Propag. (EuCAP), 2010 Proc. Fourth Eur. Conf., 2010.
[20] K.V. Deligkaris, Z.D. Zaharis, D.G. Kampitaki, et al., Thinned planar array design using Boolean PSO with velocity mutation, IEEE Trans. Magn. 45 (2009) 1490–1493.
[21] A. Moffet, Minimum-redundancy linear arrays, IEEE Trans. Antennas Propag. 16 (Mar 1968) 172–175.
[22] D. Pearson, S.U. Pillai, Y. Lee, An algorithm for near-optimal placement of sensor elements, IEEE Trans. Inf. Theory 36 (1990) 1280–1284.
[23] C.S. Ruf, Numerical annealing of low-redundancy linear arrays, IEEE Trans. Antennas Propag. 41 (1993) 85–90.
[24] J. Dong, Q. Li, F. He, et al., Co-array properties of minimum redundancy linear arrays with minimum sidelobe level, in: ISAPE 2008 – The 8th International Symposium on Antennas, Propagation and EM Theory Proceedings, 2008, pp. 74–77.
[25] D.A. Linebarger, I.H. Sudborough, I.G. Tollis, Difference bases and sparse sensor arrays, IEEE Trans. Inf. Theory 39 (1993) 716–721.
[26] P.P. Vaidyanathan, P. Pal, Sparse sensing with co-prime samplers and arrays, IEEE Trans. Signal Process. 59 (2011) 573–586.
[27] P.P. Vaidyanathan, P. Pal, Theory of sparse coprime sensing in multiple dimensions, IEEE Trans. Signal Process. 59 (2011) 3592–3608.
[28] P.P. Vaidyanathan, P. Pal, Nested arrays: a novel approach to array processing with enhanced degrees of freedom, IEEE Trans. Signal Process. 58 (2010) 4167–4181.
[29] Piya Pal, P.P. Vaidyanathan, Nested arrays in two dimensions, part II: application in two dimensional array processing, IEEE Trans. Signal Process. 60 (2012) 4706–4718.
[30] K. Han, A. Nehorai, Improved source number detection and direction estimation with nested arrays and ULAs using jackknifing, IEEE Trans. Signal Process. 63 (2013) 6118–6128.
[31] Piya Pal, P.P. Vaidyanathan, Nested arrays in two dimensions, part I: geometrical considerations, IEEE Trans. Signal Process. 60 (2012) 4694–4705.
[32] K. Han, A. Nehorai, Wideband Gaussian source processing using a linear nested array, IEEE Signal Process. Lett. 20 (2013) 1110–1113.
[33] W.K. Ma, T.H. Hsieh, C.Y. Chi, DOA estimation of quasi-stationary signals via Khatri–Rao subspace, in: Proc. International Conference on Acoustics, Speech and Signal Processing, ICASSP, 2009, pp. 2165–2168.
[34] E. Evans, J.R. Johnson, D.F. Sun, High resolution angular spectrum estimation techniques for terrain scattering analysis and angle of arrival estimation, in: Proc. 1st ASSP Workshop Spectral Estimation, Hamilton, Ontario, Canada, 1981, pp. 134–139.

[35] B. Friedlander, A.J. Weiss, Direction finding using spatial smoothing with interpolated arrays, IEEE Trans. Aerosp. Electron. Syst. 28 (1992) 574–587.
[36] G.H. Golub, C.F. van Loan, Matrix Computations, The Johns Hopkins University Press, Baltimore, 1985, pp. 405–408, ch. 12.
[37] P. Hyberg, M. Jansson, B. Ottersten, Array interpolation and bias reduction, IEEE Trans. Signal Process. 52 (2004) 2711–2720.
[38] P. Hyberg, M. Jansson, B. Ottersten, Array interpolation and DOA MSE reduction, IEEE Trans. Signal Process. 53 (2005) 4464–4471.

Pourya Alinezhad was born in Karaj, Iran, on August 5, 1990. He received the B.Sc. degree in electronics and electrical engineering from Islamic Azad University, Karaj, in 2012, and the M.Sc. degree in electrical and communications engineering from Shahid Bahonar University, Kerman, Iran, in 2014. His research interests are in digital signal processing, phased arrays and radar signal processing.

Saeid R. Seydnejad received the B.Sc. degree in electrical engineering from Sistan and Baluchestan University, Zahedan, Iran, in 1988, the M.Sc. degree in electrical engineering from Sharif University of Technology, Tehran, Iran, in 1990, and Ph.D. degree also in electrical engineering from Imperial College of Science Technology and Medicine, London, U.K., in 1998. During 1998, he was a postdoctoral Research Fellow in the Department of Biomedical Engineering of Imperial College. He worked as a DSP Engineer for GE Power Control Systems, Toronto, Canada, in 1999. From 2000 to 2007 he was a Senior DSP Design Engineer for Nortel Networks, Ottawa, Canada working on the development of next generation of optical and wireless communication systems. During 2004 to 2006 he also worked as a part time research fellow in the Division of Medical Devices, Ottawa Heart Institute, University of Ottawa, Ottawa, Canada on bio-implant devices. He is now an associate professor in the Department of Electrical Engineering, Shahid Bahonar University, Kerman, Iran. His area of interest includes, array signal processing, wireless communication systems, neural engineering and neuroprosthetic devices.

Dariush Abbasi-Moghadam was born in Kerman, Iran on July 21, 1976. He received the B.S. degree in electrical engineering from Shahid Bahonar University of Kerman, Kerman, Iran, in 1998 and the M.Sc. and Ph.D. degree from Iran University of Science and Technology, Tehran, Iran, in 2001 and 2011, respectively, both in electrical engineering. He was with the Advanced Electronic Research Center—Iran from 2001–2003 and worked on the design and analysis of satellite communication systems. In September 2004, he joined Iranian Telecommunications Company, Tehran, as a Research Engineer. He is currently with the Department of Electrical Engineering at Shahid Bahonar University, Kerman, Iran. His research interests are in the area of wireless communications, statistical signal processing, satellite communication systems, and Power line communications.